Correlative Microscopy for Nanomanipulation of Sub-Cellular Structures

Z. Gong[†], B.K. Chen[†], J. Liu, C. Zhou, D. Anchel, X. Li, D.P. Bazett-Jones, and Y. Sun

Abstract— **Nanomanipulation under scanning electron microscopy (SEM) has been demonstrated as an enabling technique for the manipulation and characterization of nanomaterials. We recently developed nanomanipulation techniques for the extraction and identification of DNA contained within sub-nuclear locations of a single cell nucleus. In nanomanipulation of DNA, a key step is target identification through SEM-fluorescence correlative imaging. Existing image correlation techniques often require fiducial marks and/or manual feature selection or data training, which are unsuitable for DNA nanomanipulation. This paper presents an approach for correlating SEM-fluorescence microscopy images, proven effective in processing images taken under poor SEM imaging conditions imposed by the necessity of preserving DNA's biochemical integrity. The performance of the image correlation approach under different imaging conditions was quantitatively evaluated. Compared to manual correlation by skilled operators, the automated correlation approach demonstrated an order of magnitude higher speed. The SEM-fluorescence correlation approach enables targeted nanomanipulation of sub-cellular structures under SEM.**

I. INTRODUCTION

The internal organization of DNA inside a cell nucleus is structured. Disruption of the organization contributes to the aberrant read-out of the DNA's information, which causes diseases such as cancers. Evidence has suggested that the different sub-nuclear structures (e.g., nucleolus [1], nuclear bodies [2], transcription factories [3]) coordinately regulate the positioning and expression of genes.

To understand how genes co-reside around preferred sub-nuclear structures, it is essential to identify the genes located around these sub-nuclear structures. We recently developed a new technique capable of extraction and identifying genes located in the proximity of a specific sub-nuclear structure [4]. The technique involves nanomanipulation inside a scanning electron microscope (SEM) to physically extract minute amount of biomaterial from a desired location inside a cell nucleus, and biochemically amplifying and sequencing the genes contained within. We did not choose to use atomic force microscopy (AFM) [5] [6] [7] for manipulating the sub-nuclear structures because in AFM, the same AFM cantilever tip is used for both imaging and manipulation, which make simultaneous imaging and manipulation difficult, and more important can lead to DNA cross contaminations.

[†]These authors contributed equally to this work.

David Anchel and David P. Bazett-Jones are with the Genetics and Genome Biology Program, the Hospital for Sick Children, 555 University Avenue, Toronto, ON M5G 1X8, Canada

The other authors are with the Advanced Micro and Nanosystems Laboratory, University of Toronto, 5 King's College Road, Toronto, ON M5S 3G8, Canada, Email: sun@mie.utoronto.ca
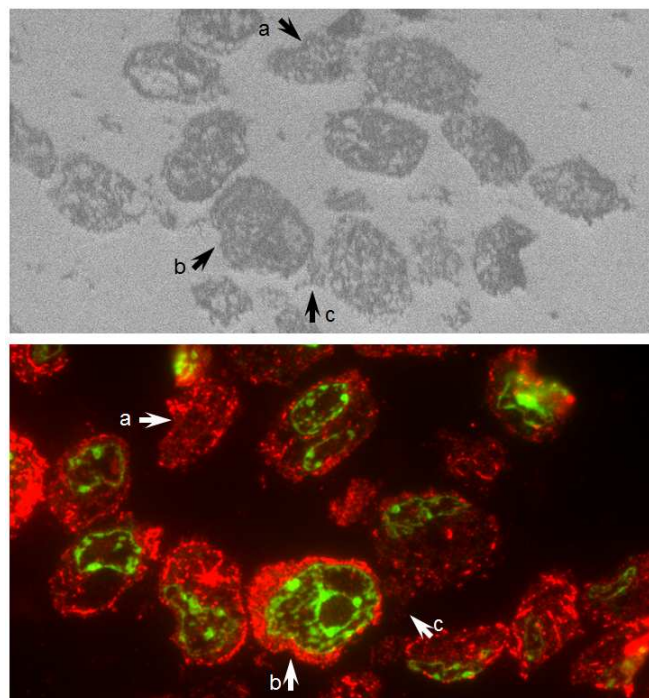
Fig. 1. Correlation between SEM and fluorescence imaging for visualizing sub-cellular structures to identify manipulation targets.

A key step in DNA extraction using nanomanipulation is to correlate SEM images with fluorescent images for identifying target of interest (Fig. 1). Fluorescence imaging permits easy visualization of sub-cellular structures, specific protein, and nucleic acid, many of which are not clearly visible in SEM imaging. In the meanwhile, SEM images provide higher imaging magnification and resolution. We conducted image correlation manually using commercially available general-purposed software; however, the process demands careful manual adjustments of image size, position, rotation, and distortions to achieve a reasonable correlation accuracy.

To improve the speed and accuracy of image correlation, image processing algorithms were developed to automatically establish correspondence between images acquired by different microscopy techniques. Correlative imaging is a challenging multi-modal and multi-scale image registration problem. The conventional microscopy image correlation techniques require the physical addition of fiducial marks to the sample as landmarks. These landmarks can be easily identified in images captured under different modes of microscopy (e.g., SEM and fluorescence) [8] [9] [10] [11]. However, our DNA extraction task must be conducted under
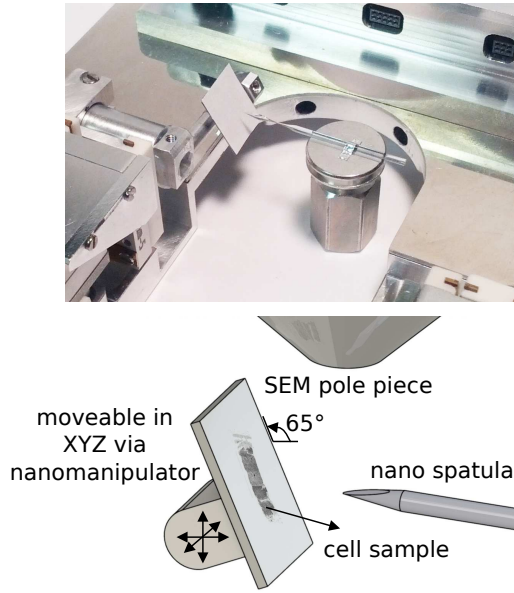
Fig. 2. DNA nanomanipulation setup inside SEM. Cell sample is mounted on an XYZ nanomanipulator, facing the stationary end tool (nano spatula).
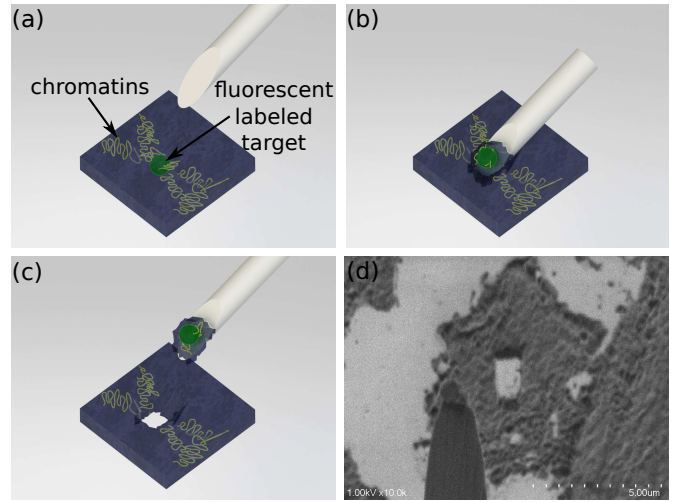

Fig. 3. DNA extraction from within a single cell nucleus. (a) Locating the cell of interest inside SEM, guided by correlated fluorescent image (not shown). (b) Landing the nano spatula tip onto the target of interest, and slide the cell fragments onto the beveled surface. (c) Lifting up the nano spatula along with the extracted cell fragment. (d) SEM image taken after DNA extraction. The SEM images were taken under higher electron energy (1kV) and slower scan rate to enhance image quality. In reality, lower electron energy is used (0.4kV) to ensure survival of DNA.

specific SEM imaging conditions with limited imaging resolution, imposed by the necessity of preserving the biochemical integrity of the sample. This poor imaging condition makes the identification of nanometer-sized fiducial marks difficult. Although methods also exist requiring no fiducial marks [12] [13] for image correlation, these methods are time consuming due to heavy manual inventions required (e.g., manually select features, data training etc.), or require special reference marks on the sample substrate.

To cope with translation, rotation, and scaling differences between images, scale invariant feature transform (SIFT) descriptor [14] is a powerful technique for detecting a set of local feature vectors for image registration. Mikolajczyk et al. evaluated the performance of various local invariant feature descriptors and concluded that the SIFT descriptor outperformed other descriptors [15]. The SIFT algorithm, however, cannot extract the affine transformed (i.e., distorted) features. This challenge was overcome by the fully affine invariant SIFT (ASIFT) approach [16], with the drawback of significantly more computationally demanding than SIFT.

In this paper, the ASIFT algorithm is used to correlate SEM and fluorescent images for identifying sub-cellular structures. It was accelerated by graphic processing unit (GPU) to enhance the speed and accuracy of SEM-fluorescence image correlation. The correlation results under different imaging conditions were quantitatively evaluated. The suitability of the approach for SEM-based nanomanipulation of sub-cellular structures is discussed.

II. DNA NANO-EXTRACTION

For the completeness of this paper, a brief overview of our DNA nanomanipulation process is introduced in this section. In sample preparation, cells are sliced into thin cross sections using cryomicrotome, and its fluorescent images are taken. After transferring the sample into SEM, the fluorescent images are correlated with the SEM images to identify targets of interest for manipulation. Fig. 2 shows the nanomanipulation setup inside SEM. Cell sample is mounted on the nanomanipulator, which provides close-looped, nanometer motion resolution along XYZ axes [17]. The custom fabricated end tool, termed nano spatula, is mounted horizontally on a stationary support, facing the slanted sample substrate. The nanomanipulation system and the nano spatula are controlled to physically 'scoop up' the target within a single cell nucleus (Fig. 3). Finally, the extracted material is removed from the SEM, amplified by polymerase chain reaction and sequenced to identify the genes.

To minimize electron beam damage to DNA, the accelerating voltage of SEM imaging must be kept low, at the expense of significantly increasing SEM image noise level. Moreover, the cell sample is tilted to minimize electron penetration depth into the sample, which causes distortions to SEM images. Image distortion caused by sample tilting can be largely compensated by the SEM itself; however, this requires accurate knowledge of sample tilting angles. In standard SEM imaging, sample tilting angle is estimated via manual trial and error.

The necessary low accelerating voltages and sample tilting, for preserving the integrity of DNA during SEM imaging and nanomanipulation, result in noisy and distorted images. In addition, cells' fluorescent images are taken in the wet state, while the SEM images are taken in the dry vacuum environment. Experimental observation reveal that the cell sample shrinks inside SEM (vs. wet state under fluorescence imaging). This complication further distorts the images.
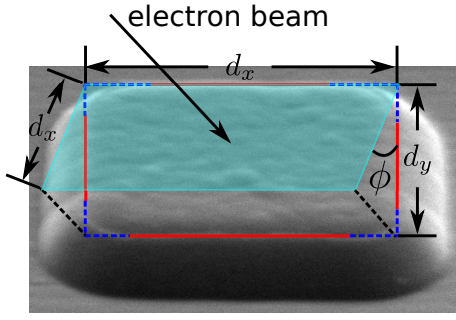
Fig. 4. Sample tilting angle estimation under SEM imaging.

III. SEM-Fluorescence Image Correlation

This section describes an image correlation procedure developed for nano-extraction of DNA. The first step is to estimate the cell sample tilting angle. It is input into the SEM to automatically compensate for most of the image distortions caused by sample tilting. SEM images are then denoised in real-time using GPU accelerated non-local (NL) means [18] filtering and are correlated with fluorescent images using the ASIFT method.

A. Estimation of sample tilting angle

Most SEMs has an integrated function to compensate for image distortions caused by sample tilting, given that the tilting angle is accurately known. For each DNA nanomanipulation experiment, the sample tilting angle varies slightly due to mechanical misalignments of the setup. For calibration, a sample containing micrometer-sized reference object (square shown in Fig. 4) is placed adjacent to the cell sample. Depending upon the tilting angle (ϕ) of the cell sample, the sides of the square reference would appear shorter in proportion according to trigonometry. Because the SEM image is nearly an orthogonal parallel projection [19], the tilting angle is $\phi = \arccos \frac{d_y}{d_x}$. Using Canny edge detection and Hough transform, lines are detected and colored in red shown in Fig. 4.

B. Image denoising

The NL-means algorithm [20] filters a noisy image $v(i)$ by computing a weighted average of all the pixels in a search window.

$$NL[v](i) = \sum_{j \in I} \frac{1}{Z(i)} e^{-\frac{\|v(\mathcal{N}_i) - v(\mathcal{N}_j)\|_{2,\alpha}^2}{h^2}} v(j) \qquad (1)$$

In our previous work [18], we demonstrated that as a preprocessing step for SEM image analysis, NL-means filtering outperforms other popular denoising algorithms. In this work, we apply NL-means filtering to SEM images before performing image registration for increasing image correlation accuracy.

C. Image registration

The ASIFT algorithm introduces an affine model to the SIFT descriptor for effective extraction of distorted image features. Assuming image distortions are caused by viewpoint changes, image distortions can be locally expressed by affine planar transforms [16]. The deformation model of image $u(x,y)$ is $u(x,y) \rightarrow u(ax + by + e, cx + dy + f)$. $A = \begin{bmatrix} a & b \\ c & d \end{bmatrix}$ is a linear planar map having the following decomposition

$$A = \lambda \begin{bmatrix} \cos\alpha & -\sin\alpha \\ \sin\alpha & \cos\alpha \end{bmatrix} \begin{bmatrix} \phi & 0 \\ 0 & 1 \end{bmatrix} \begin{bmatrix} \cos\beta & -\sin\beta \\ \sin\beta & \cos\beta \end{bmatrix} \qquad (2)$$

where α denotes the rotation angle and λ is the scale factor, both of which can be estimated with the SIFT algorithm. ϕ is latitude angle and β is longitude angle, and the two define the imaging axis orientation.

The ASIFT algorithm involves two steps. Firstly, an image pair (one SEM image and one fluorescent image) to be registered is individually transformed by simulating a large set of linear distortions caused by the change of the longitude angle β and latitude angle ϕ. Secondly, it performs SIFT comparison of all the simulated images generated to find correct matching features. Since every three pairs of matching point features determines a unique affine transformation, least squares fit is used to compute a refined affine transformation. With the computed affine transformation, our system overlays the fluorescent image on top of SEM image to identify the target region in the SEM image.

For a typical SEM image with a size of 640×480, the traditional CPU implementation of ASIFT algorithm costs more than two minutes. We accelerated this computation via GPU since the the problem can be expressed as data-parallel computations. The first step of ASIFT, simulating distortions by varying imaging axis, can be fully parallelized because the transformations applied to the different pixels are mutually independent. The second step of ASIFT, although not parallelized in nature, can still be accelerated by exploiting GPU memory architectures such as shared memory.

D. Correlation accuracy evaluation

Mean absolute error (MAE) is used in this work to measure the accuracy of image correlation with the ASIFT algorithm. In manual benchmarking, a skilled operator carefully aligns a large number of features over the entire image (vs. using a few feature points only). Manual alignment parameters such as rotational angles and scaling ratios are recorded and used to create an affine transformation matrix. Each feature point in the SEM image is transformed onto the corresponding fluorescent image using both the benchmarking matrix and the matrix produced by the ASIFT method. MAE is then determined by averaging all the errors.

IV. Experimental Results

A. Tilt angle estimation

A calibration sample that contains micrometer-sized square features was used to evaluate the effectiveness of sample tilt angle estimation. The dimensions of a tilted square were measured through SEM imaging, and the sample tilting angle was estimated via the method described in
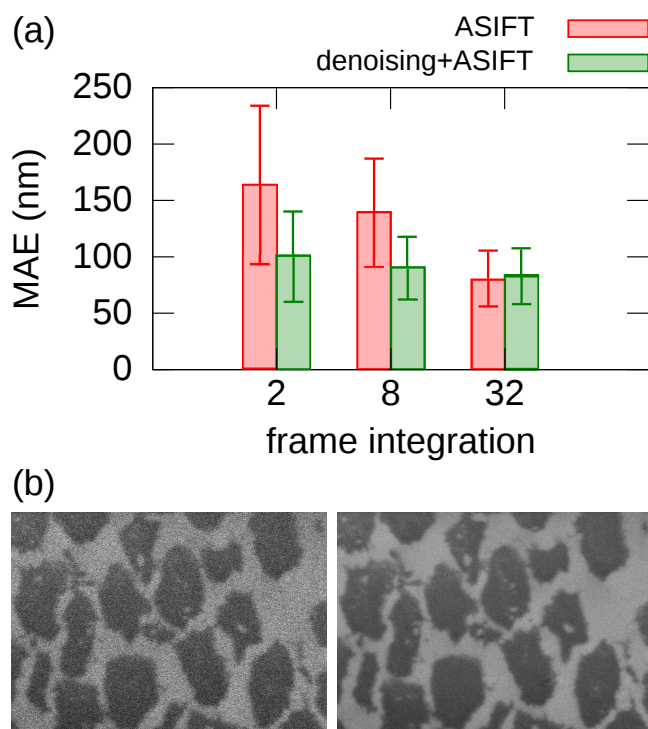
Fig. 5. (a) Effect of image noise level on correlation accuracy. The highest frame rate of the SEM is ∼20Hz; thus, 2 frames integration corresponds to 10Hz frame rate. Under each frame integration setting, ten SEM-fluorescence image pairs were computed, and the error bars represent ±1 standard deviation. (b) A sample SEM image taken with 2 frames integration, before denoising (left) and after denoising (right).
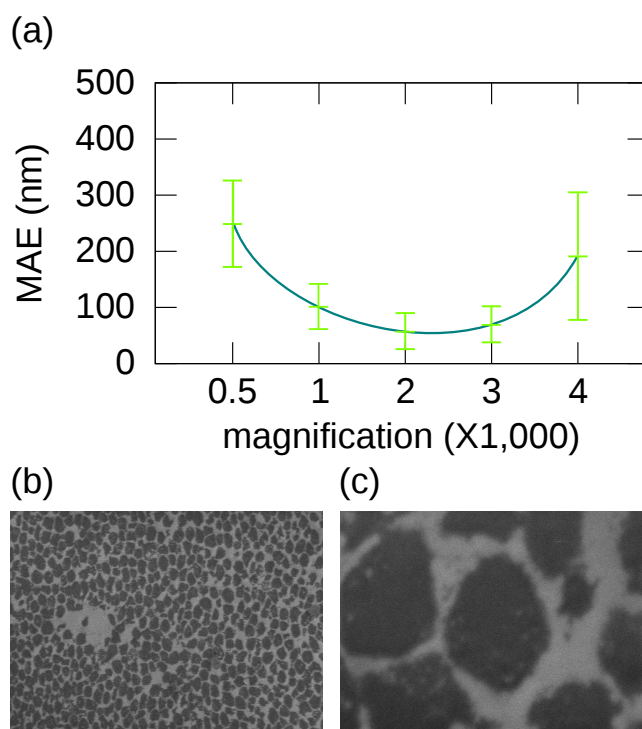

Fig. 6. (a) Correlation accuracy under different SEM imaging magnifications. (b) and (c) represent two SEM magnification extremes, where ASIFT was found to have difficulty in identifying matching features needed for image correlation.

Section III-A. The distortion compensated image based on the estimated sample tilting angle was compared to the actual dimensions of the square feature, measured from the top view. The differences in the square's side length were within 10 pixels (corresponds to ∼±2.5 degrees sample tilt). This effective distortion compensation significantly facilitates SEM-fluorescence image correlation.

B. Correlation Accuracy

The correlation accuracy is quantified through MAE, as described in Section III-D. Two main factors influence the image correlation accuracy, including SEM image noise level and SEM magnification. Fluorescent images were taken at the highest magnification and had inheritably low noise level.

1) Image noise level vs. correlation accuracy: Fig. 5 shows quantitatively how different noise levels in SEM imaging affect image correlation accuracy. Different SEM image noise levels were simulated by choosing different amounts of image frame integration. With higher frame integration, the frame rate became lower. Lower frame rates results in lower noise levels. As shown in Fig. 5, the accuracy of image registration is highly dependent upon the noise level of SEM images.

For nano-extraction of DNA inside SEM, high frame rates (i.e., lower frame integration) allow more real-time and better visualization of the nanomanipulation process. To improve the correlation accuracy at high frame rates, the system per-

forms NL-means denoising pre-processing on SEM images before correlation is made. This pre-processing step was found to significantly improve the MAE of correlation at high SEM frame rates. In experiments, nanomanipulation was typically conducted under 10Hz SEM imaging (i.e., 'frame integration' = 2 in Fig. 5(b)). In this case, NL-means denoising improved the MAE of SEM-fluorescence image correlation by 62%, compared to directly performing correlation without denoising SEM images. At low frame rates (e.g., 32 frames integrated), little noise existed; hence, the denoising algorithm undesirably reduced image contrast slightly on these low-noised SEM imgaes, resulting in slightly reduced correlation accuracy.

2) Image magnification vs. correlation accuracy: Since image magnification affects the number of identifiable features in the field of view, it plays a key role in the accuracy of SEM-fluorescence image registration. Under each SEM imaging magnification, ten random regions of the cell sample were correlated with its corresponding fluorescent images, and the correlation accuracy was computed and summarized in Fig. 6(a). The results show that correlation accuracy (i.e., reduced MAE) increased with image magnification, up until a magnification of ∼2,400X, after which the trend reversed.

Under the SEM imaging conditions that ensure low electron beam-induced DNA damage, only the cell membrane contour is easily visible in SEM images. As the image magnification increases, the cell membrane contour becomes better defined from the increase in image resolution, at the expense that the number of cells within the field of view
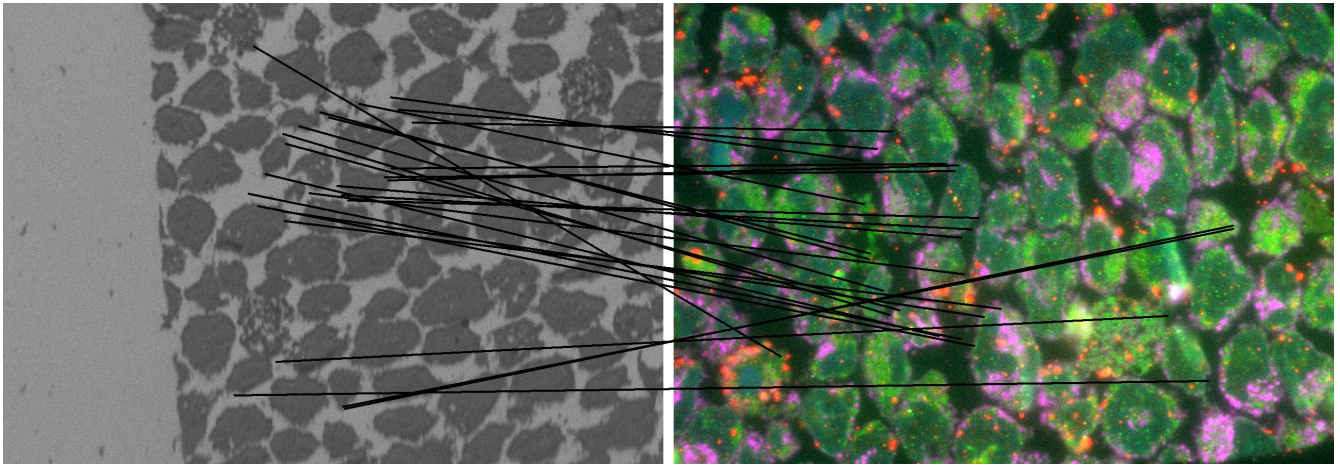
Fig. 7. SEM and fluorescent images. Black lines connect the identified matching feature points.

decreases. At magnifications lower than 2,400X, the effect of higher image resolution outweighs the loss in having fewer cells/features within the field of view. Therefore, the correlation accuracy improves with increase in magnification. This trend reverses at magnifications higher than 2,400X because the actual SEM imaging resolution under the poor, DNA viable imaging conditions does not longer improve essentially. In the meanwhile, the number of cells in the field of view continues to decrease at higher magnifications, reducing the number of identifiable features.

Image correlation failure occurred at the two magnification extremes. For magnification <500X (Fig. 6(b)), the poor imaging resolution often does not provide an adequate number of identifiable features for completing the affine transformation (Eq. 2). At the other extreme, with magnifications >4,000X (Fig. 6(c)), the number of features within the field of view again became too low to achieve a high correlation accuracy.

C. Efficiency of GPU accelerated ASIFT

During the process of DNA extraction, several factors caused SEM imaging to drift over time. These factors include external electromagentic interferences, sample negative charging, and thermal drift of the nanomanipulator. This drift in SEM imaging makes the image correlation process time sensitive, demanding the completion of image correlation quickly. If the computation of ASIFT takes too long, the transformed fluorescent image would not overlay well with the live video feed from the SEM.

GPU parallel computing was utilized in our system to speed up the computation of ASIFT. The GPU accelerated ASIFT correlation was implemented on a standard PC (Intel Core i7 3.6GHz CPU, 3GB DDR3 RAM, NVidia GTX560 GPU with 1GB global memory and 48kB on-chip shared memory per block). For correlation of image pairs that are 640×480 pixels in size, the GPU accelerated ASIFT took an average of $15.3 \pm 5.7s$ to correlate one image pair (n=20). This speed is approximately nine times faster than CPU correlation (averagely $140.5 \pm 30.3s$ per correlation),
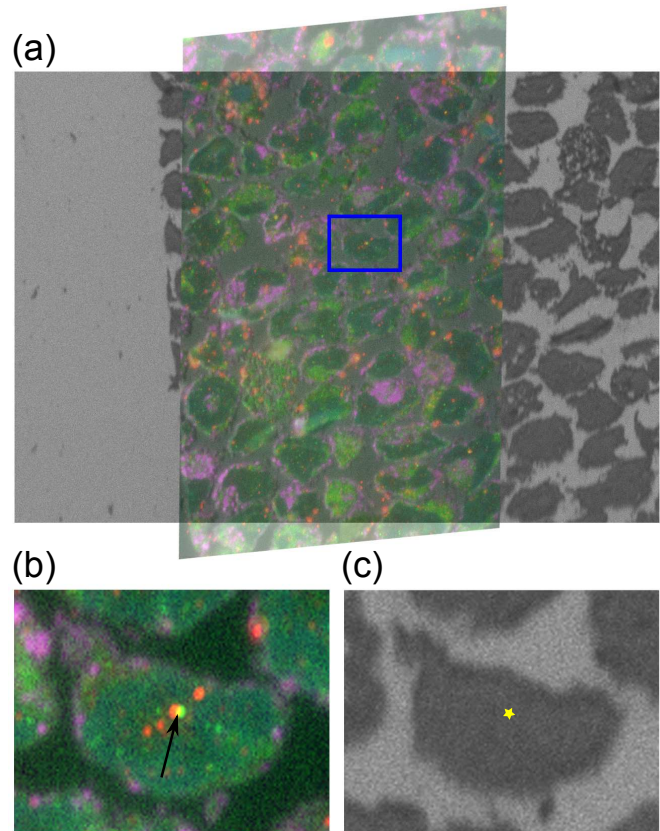

Fig. 8. (a) Overlaid SEM and fluorescent images at low magnification. Zooming into a single cell level reveals well correlated features between (b) fluorescent image and (c) SEM image.

and about 11 times higher than manual operation (averagely $174.9 \pm 56.4s$ per correlation). The average drift rate of our nanomanipulation setup was $1.24nm/s$, determined with the method we previously reported [17]. With GPU accelerated ASIFT, a $15.3s$ computation time translates to SEM image drift of $\sim 19nm$.

D. Image correlation for DNA extraction

Fig. 7 and Fig. 8 illustrate examples of SEM-fluorescence image correlation results. The SEM images were taken under SEM conditions that ensure DNA viability, at a frame rate of 10Hz. They were denoised in real time by GPU accelerated NL-means filtering. The fluorescent images were converted to grayscale image followed by intensity inversion. Fig. 7 shows the registration of the images, where the black lines connect matching feature points in the SEM and fluorescent images. Fig. 8 shows the transformed fluorescent image overlaid on top of the SEM image. Zooming into a single cell level shows well correlated images (Fig. 8(b),(c)). From fluorescence imaging, the location of manipulation target is the overlapping region between the red and green fluorescent spots (NB4 cell nuclear body, $\sim 0.8 \mu m$ in size) in Fig. 8(b) (arrow labeled). The corresponding location in the SEM image is shown in Fig. 8(c). The MAE value was quantified to be $89nm$, which is the accuracy of SEM-fluorescence correlation of this image pair.

V. Conclusion

In SEM-based nanomanipulation of biomaterials within sub-cellular structures, electron beam induced damage to the biomaterials such as DNA must be minimized in order to preserve their biochemical integrity. The SEM imaging conditions suitable for this purpose, however, result in noisy and distorted images. This paper described the use of NL-means denoising and ASIFT image correlation for locating a target of interest within SEM and fluorescent images. Through accelerated GPU implementations of the algorithms, denoising of SEM images was achieved in real time, and image correlation was shown to be eleven times faster than manual operation. Various factors influencing the performance of the proposed SEM-fluorescence image correlation process were evaluated. Our SEM-fluorescence correlation approach requires no fiducial marks and no manual feature selection or data training, enabling targeted nanomanipulation of sub-cellular structures under SEM.

References

[1] T. M. Yusufzai, H. Tagami, Y. Nakatani, and G. Felsenfeld, "{CTCF} tethers an insulator to subnuclear sites, suggesting shared insulator mechanisms across species," *Molecular Cell*, vol. 13, no. 2, pp. 291 – 298, 2004.

[2] S. Schoenfelder, T. Sexton, L. Chakalova, N. F. Cope, A. Horton, S. Andrews, S. Kurukuti, J. A. Mitchell, D. Umlauf, D. S. Dimitrova, C. H. Eskiw, Y. Luo, C.-L. Wei, Y. Ruan, J. J. Bieker, and P. Fraser, "Preferential associations between co-regulated genes reveal a transcriptional interactome in erythroid cells," *Nature Genetics*, vol. 42, no. 1, pp. 53–61, 2009.

[3] C. Osborne and C. Eskiw, "Where shall we meet? a role for genome organisation and nuclear sub-compartments in mediating interchromosomal interactions." *Journal of Cellular Biochemistry*, vol. 104, no. 5, pp. 1553–1561, 2008.

[4] B. K. Chen, D. Anchel, Y. Sun, and D. P. Bazett-Jones, "Nanodissection and identification of gene loci from single cells." September 2013, submitted to *Nature Methods*.

[5] H. G. Hansma, J. Vesenka, C. Siegerist, G. Kelderman, H. Morrett, R. L. Sinsheimer, V. Elings, C. Bustamante, and P. K. Hansma, "Reproducible imaging and dissection of plasmid dna under liquid with the atomic force microscope," *Science*, vol. 256, no. 5060, pp. 1180–1184, 1992.

[6] J. Hu, Y. Zhang, H. Gao, M. Li, and U. Hartmann, "Artificial dna patterns by mechanical nanomanipulation," *Nano Letters*, vol. 2, no. 1, pp. 55–57, 2002.

[7] J. Lü, H. An, H. Li, X. Li, Y. Wang, M. Li, Y. Zhang, and J. Hu, "Nanodissection, isolation, and pcr amplification of single dna molecules," *Surface and Interface Analysis*, vol. 38, no. 6, pp. 1010–1013, 2006.

[8] B. G. Kopek, G. Shtengel, C. S. Xu, D. A. Clayton, and H. F. Hess, "Correlative 3d superresolution fluorescence and electron microscopy reveal the relationship of mitochondrial nucleoids to membranes," *Proceedings of the National Academy of Sciences*, vol. 109, no. 16, pp. 6136–6141, 2012.

[9] W. Kukulski, M. Schorb, S. Welsch, A. Picco, M. Kaksonen, and J. A. G. Briggs, "Correlated fluorescence and 3d electron microscopy with high sensitivity and spatial precision," *The Journal of cell biology*, vol. 192, no. 1, pp. 111–119, 2011.

[10] S. Watanabe, A. Punge, G. Hollopeter, K. I. Willig, R. J. Hobson, M. W. Davis, S. W. Hell, and E. M. Jorgensen, "Protein localization in electron micrographs using fluorescence nanoscopy," *Nature Methods*, vol. 8, no. 1, pp. 80–84, 2010.

[11] D. N. Fronczek, C. Quammen, H. Wang, C. Kisker, R. Superfine, R. Taylor, D. A. Erie, and I. Tessmer, "High accuracy fiona-afm hybrid imaging," *Ultramicroscopy*, vol. 111, no. 5, pp. 350–355, 2011.

[12] T. Cao, T. Zach, S. Modla, D. Powell, K. Czymmek, and M. Niethammer, "Registration for correlative microscopy using image analogies," in *Proceedings of the 5th international conference on Biomedical Image Registration*, 2012, pp. 296–306.

[13] S. Halary, S. Duperron, and T. Boudier, "Direct image-based correlative microscopy technique for coupling identification and structural investigation of bacterial symbionts associated with metazoans," *Applied and Environmental Microbiology*, vol. 77, no. 12, pp. 4172–4179, 2011.

[14] D. G. Lowe, "Distinctive image features from scale-invariant keypoints," *Int. J. Comput. Vision*, vol. 60, no. 2, pp. 91–110, Nov. 2004.

[15] K. Mikolajczyk and C. Schmid, "A performance evaluation of local descriptors," *IEEE Trans. Pattern Anal. Mach. Intell.*, vol. 27, no. 10, pp. 1615–1630, 2005.

[16] J.-M. Morel and G. Yu, "Asift: A new framework for fully affine invariant image comparison," *SIAM J. Img. Sci.*, vol. 2, no. 2, pp. 438–469, Apr. 2009.

[17] Y. L. Zhang, Y. Zhang, C. Ru, B. K. Chen, and Y. Sun, "A load-lock-compatible nanomanipulation system for scanning electron microscope," *IEEE/ASME Transactions on Mechatronics*, vol. PP, no. 99, pp. 1 –8, 2011.

[18] Z. Gong, B. K. Chen, J. Liu, and Y. Sun, "Robotic probing of nano structures inside scanning electron microscopy," *IEEE Transactions on Robotics*, accepted for publication, 2014.

[19] E. Schönherr and E. Winckler, "A sample holder for measuring the interfacial angles of small crystals using a scanning electron microscope," *Journal of Crystal Growth*, vol. 36, no. 2, pp. 353 – 354, 1976.

[20] A. Buades, B. Coll, and J.-M. Morel, "A non-local algorithm for image denoising," in *Computer Vision and Pattern Recognition, 2005. CVPR 2005. IEEE Computer Society Conference on*, vol. 2, june 2005, pp. 60 – 65.